Article

Synthesis of Tetrahedral LiFeO and Its Behavior as a Cathode in Rechargeable Lithium Batteries

A. Robert Armstrong, Daniel W. Tee, Fabio La Mantia, Petr Novk, and Peter G. Bruce

J. Am. Chem. Soc., **2008**, 130 (11), 3554-3559 • DOI: 10.1021/ja077651g

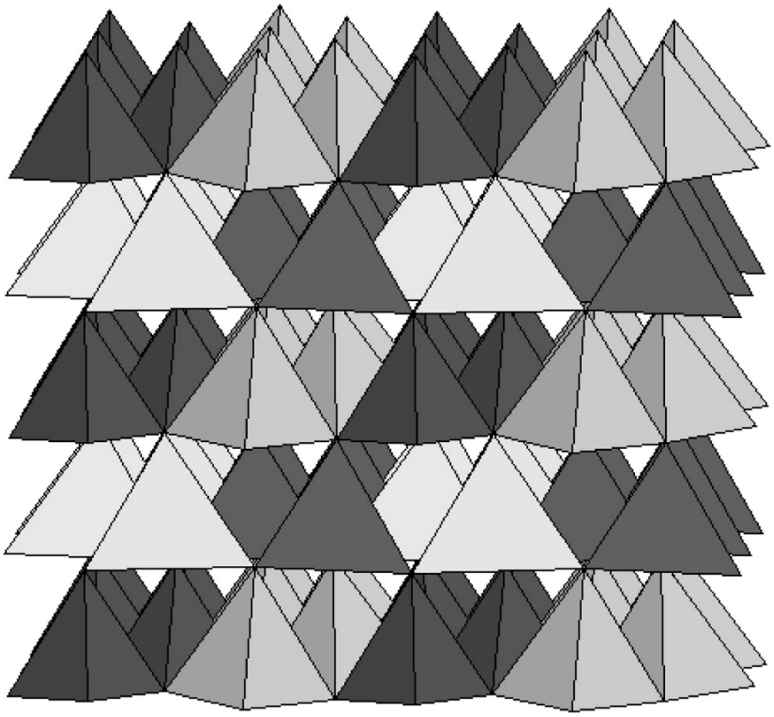

J|A|C|S
ARTICLES
Published on Web 02/20/2008

Synthesis of Tetrahedral $LiFeO_2$ and Its Behavior as a Cathode in Rechargeable Lithium Batteries

A. Robert Armstrong,[†] Daniel W. Tee,[†] Fabio La Mantia,[‡] Petr Novák,[‡] and Peter G. Bruce*,[†]

EaStCHEM, School of Chemistry, University of St. Andrews, St. Andrews, Fife, KY16 9ST, UK, and Paul Scherrer Institut, Electrochemistry Laboratory, CH-5232 Villigen PSI, Switzerland

Received October 10, 2007; E-mail: pgb1@st-and.ac.uk

Abstract: Synthesis and structural characterization of the first $LiFeO_2$ compound with tetrahedrally coordinated Fe^{3+} is reported. When used as a positive intercalation electrode in a lithium cell, it can store charge of up to 120 $mAhg^{-1}$ at a rate of 100 mAg^{-1}. However, it converts to the defect spinel $LiFe_5O_8$ on cycling. By combining results from powder X-ray diffraction, differential electrochemical mass spectrometry, electrochemical cycling, and TG-MS, it is shown that such conversion, which involved oxygen loss, is not associated with direct O_2 gas evolution but instead reaction with the electrolyte. We suggest that intercalation/deintercalation is accompanied by the exchange of Li^+ by H^+ in the material and subsequent loss of H_2O, thus converting $LiFeO_2$ to the defect spinel $LiFe_5O_8$ on cycling.

Introduction

Lithium intercalation compounds with the composition $LiFeO_2$ are potentially very attractive cathodes for rechargeable lithium batteries because of their much lower cost and toxicity (relationship to rust) compared with $LiCoO_2$ used in the vast majority of present day cells.[1−4] Previous studies of $LiFeO_2$ compounds have all focused on polymorphs containing octahedrally coordinated Fe^{3+}, including the layered analogue of $LiCoO_2$,[5−7] a corrugated layered phase,[8,9] and other polymorphs such as those based on the ramsdellite and hollandite structures.[10−14] None of these compounds have proven to be stable when used as cathodes nor capable of supporting extended cycling. Complementing these studies, there is of course a great deal of interest in iron compounds containing complex oxoanions such as $LiFePO_4$.[15−20] Here, we report the first synthesis of a $LiFeO_2$ compound with tetrahedrally coordinated Fe^{3+} and describe its properties as an intercalation electrode. It can deliver a capacity to store charge of 120 $mAhg^{-1}$ at a rate of 100 mAg^{-1}. Intercalation/deintercalation of lithium is accompanied by a phase transformation to the defect spinel structure $LiFe_5O_8$. Differential electrochemical mass spectrometry reveals little evidence that the associated oxygen loss occurs by direct O_2 evolution. We suggest that the formation of $LiFe_5O_8$ occurs by electrolyte oxidation, H^+ insertion, and H_2O loss.

Experimental Section

The parent phase, β-$NaFeO_2$, was prepared by conventional solid-state synthesis involving mixing Na_2CO_3 (Fisher, 99.5%; 5% excess by weight) and Fe_2O_3 (Aldrich, 99%) and firing at 900 °C for 12 h in air. The lithium phase was synthesized by an ion exchange process involving refluxing with a 10-fold excess of LiCl (Aldrich, 99%) in dry *n*-hexanol (Aldrich, 99%) at 160 °C. Typically, two ion exchanges, each lasting 8 h, were required to achieve complete exchange. To investigate the effects of particle size, the sodium phase was ball-milled (SPEX Centri-Prep 8000M mixer/mill) for up to 2 h. Sodium phases that were ball-milled for 2 h could be ion-exchanged in a single 8 h step.

Powder X-ray diffraction was performed on a Stoe STADI/P diffractometer operating in transmission mode with $FeK_{\alpha 1}$ radiation. Time-of-flight powder neutron diffraction data were collected on the GEM high intensity, medium-resolution instrument at ISIS, Rutherford Appleton Laboratory. The structures were refined by the Rietveld

[†] University of St. Andrews.
[‡] Paul Scherrer Institut.

(1) Whittingham, M. S. *Chem. Rev.* **2004**, *104*, 4271.
(2) Aricò, A. S.; Bruce, P. G.; Scrosati, B.; Tarascon, J.-M.; van Schalkwijk, W. *Nature Mater.* **2005**, *4*, 366.
(3) *Advences in Lithium-Ion Batteries*; van Schalkwijk, W. A., Scrosati, B., Eds.; Kluwer Academic/Plenum Publishers: New York, 2002.
(4) *Lithium Batteries Science and Technology*; Nazri, G.-A., Pistoia, G., Eds.; Kluwer Academic Publishers: Boston, 2004.
(5) Fuchs, B.; Kemmler-Sack, S. *Solid State Ionics* **1994**, *68*, 279.
(6) Tabuchi, M.; Ado, K.; Sakaebe, H.; Masquelier, C.; Kageyama, H.; Nakamura, O. *Solid State Ionics* **1995**, *79*, 220.
(7) Shirane, T.; Kanno, R.; Kawamoto, Y.; Takeda, Y.; Takano, M.; Kamiyama, T.; Izumi, F. *Solid State Ionics* **1995**, *79*, 227.
(8) Kanno, R.; Shirane, T.; Inaba, Y.; Kawamoto, Y. *J. Power Sources* **1997**, *68*, 145.
(9) Sakurai, Y.; Arai, H.; Okada, S.; Yamaki, J. *J. Power Sources* **1997**, *68*, 711.
(10) Bordet-Le-Guenne, L.; Deniard, P.; Lecerf, A.; Biensan, P.; Siret, C.; Fournès, L.; Brec, R. *J. Mater. Chem.* **1999**, *9*, 1127.
(11) Amine, K.; Yasuda, H.; Yamachi, M. *J. Power Sources* **1999**, *81−82*, 221.
(12) Matsumura, T.; Kanno, R.; Inaba, Y.; Kawamoto, Y.; Takano, M. *J. Electrochem. Soc.* **2002**, *149*, A1509.
(13) Lee, Y. S.; Cho, S. J.; Sun, Y. K.; Kobayakawa, K.; Sato, Y. *Electrochem.* **2005**, *73*, 874.
(14) Kim, J.; Manthiram, A. *J. Electrochem. Soc.* **1999**, *146*, 4371.
(15) Padhi, A. K.; Nanjundaswamy, K. S.; Goodenough, J. B. *J. Electrochem. Soc.* **1997**, *144*, 1188.
(16) Padhi, A. K.; Nanjundaswamy, K. S.; Masquelier, C.; Okada, S.; Goodenough, J. B. *J. Electrochem. Soc.* **1997**, *144*, 1609.
(17) Yamada, A.; Chung, S. C.; Hinokuma, K. *J. Electrochem. Soc.* **2001**, *148*, A224.
(18) Chung, S. Y.; Bloking, J. T.; Chiang, Y. M. *Nature Mater.* **2002**, *1*, 123.
(19) Herle, P. S.; Ellis, B.; Coombs, N.; Nazar, L. F. *Nature Mater.* **2004**, *3*, 147.
(20) Delacourt, C.; Poizot, P.; Tarascon, J. M.; Masquelier, C. *Nature Mater.* **2005**, *4*, 254.

10.1021/ja077651g CCC: $40.75

method using the program *Prodd* based on the Cambridge Crystallographic Subroutine Library (CCSL).[21] Neutron scattering lengths of −0.19, 0.945, and 0.5803 (all $\times 10^{-12}$ cm) were assigned to lithium, iron, and oxygen, respectively.[22]

Transmission electron microscopy was performed on a Jeol JEM-2011 instrument. BET measurements were carried out using a Hiden IGA porosimeter. Electrochemical properties were measured on electrodes prepared using mixtures comprising 75% active material, 18% Super S carbon, and 7% PTFE, dry mixed, and pressed into pellets. Electrodes for combined thermogravimetric analysis/mass spectrometry (TG-MS) measurements were prepared by mixing active material with graphite in the weight ratios 83:17 and then cold pressing. The cells consisted of the composite electrode, a lithium metal counter/reference electrode, and the electrolyte, a 1 molal solution of $LiPF_6$ in ethylene carbonate/dimethyl carbonate 1:1 (v/v (Merck)). All of the cells were constructed and handled in an Ar filled MBraun glovebox. Electrochemical measurements were carried out at 30 °C using a Biologic MacPile II system or a Maccor battery cycler. Combined TG-MS measurements were performed using a Netzsch STA449 Jupiter instrument coupled with a Pfeiffer Vacuum Thermostar GSD300T. The TGA heating rate was 5 °C min^{-1} up to 500 °C under an argon atmosphere.

In situ differential electrochemical mass spectrometry (DEMS) analysis was carried out to detect the gases generated during charge/discharge. The cell consisted of a lithium anode, electrolyte (as above), and the working positive electrode. The latter was formed by casting a mixture of the active material, Super S carbon, and Kynar Flex 2801 binder in NMP in the weight ratios 75:15:10 on the titanium current collector and drying at 120 °C overnight. The cell was purged continuously with argon gas, which flowed from the cell into the mass spectrometer carrying the evolved gases for MS analysis. The experiment setup is described in detailed elsewhere.[23−24]

Results and Discussion

Synthesis and Structure of T−$LiFeO_2$. The synthesis of $LiFeO_2$ with tetrahedrally coordinated cations (hereafter denoted T−$LiFeO_2$) could not be carried out directly but was achieved by first preparing tetrahedral β-$NaFeO_2$ and then exchanging Na^+ with Li^+, as described in the Experimental Section. PXRD data for both the sodium and lithium phases are shown in part a of Figure 1, where, despite the expected change in lattice parameters and some peak broadening, after ion exchange, it is clear that the structure has been retained.

$NaFeO_2$ exists in two tetrahedral structures, designated β and γ; the β polymorph was employed as a model with which to refine the structure of $LiFeO_2$ using the Rietveld method and powder neutron diffraction data, (Supporting Information).[25] The crystallographic parameters and view of the refined structure are presented in Table 1 and part b of Figure 1, respectively. When the lithium site occupancy was allowed to vary, it refined to unity to within 1 esd, thus confirming the completeness of the ion exchange. From part b of Figure 1, it is evident that the crystal structure consists of tetragonally packed O^{2-} ions (a distorted form of hexagonal close packing in which the coordination number of O^{2-} is reduced from 12 to 11).[26] The lithium and iron ions occupy half of the tetrahedral sites between

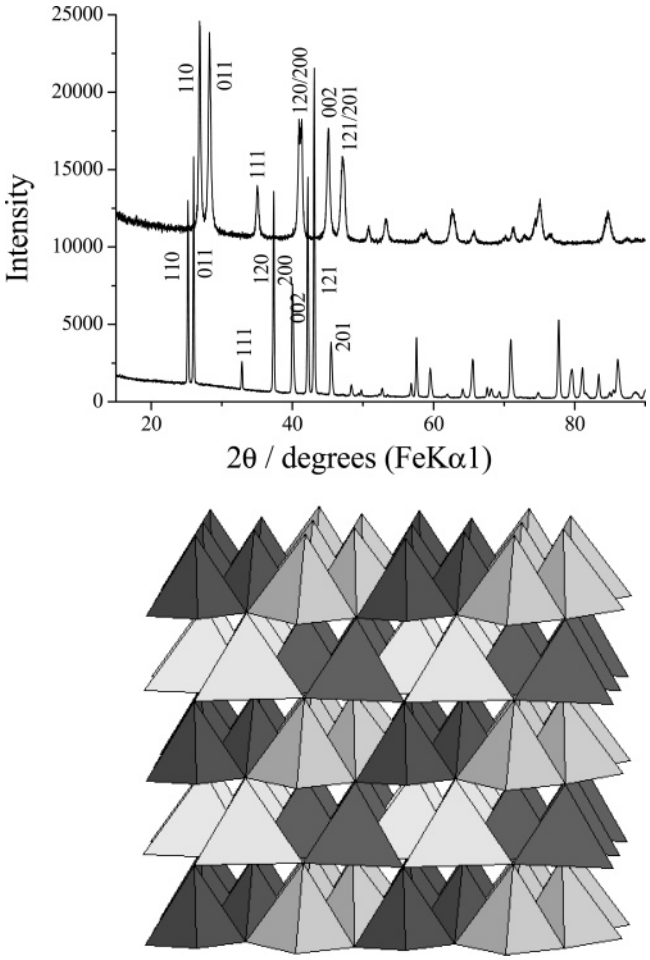

Figure 1. a. Powder X-ray diffraction patterns for β-$NaFeO_2$ (lower) and T−$LiFeO_2$ (upper). b. View of the T−$LiFeO_2$ structure. Dark tetrahedra, FeO_4; light, LiO_4.

Table 1. Refined Crystallographic Parameters for T−$LiFeO_2$[a]

atom	Wyckoff symbol	*x*/*a*	*y*/*b*	*z*/*c*	B_{iso}
Li	4a	0.413(3)	0.198(3)	0.546(3)	0.2(3)
Fe	4a	0.077(1)	0.1169(5)	0.0	0.05(5)
O1	4a	0.067(2)	0.1338(12)	0.3580(12)	2.8(2)
O2	4a	0.421(2)	0.1535(10)	0.8908(8)	0.63(12)

[a] Space group $Pna2_1$ (33); a = 5.5160 (9) Å, b = 6.4139 (12) Å, c = 5.0789 (5) Å; R_{exp} = 3.2%, R_{wP} = 5.7%, R_P = 5.0%

the O^{2-} ions, such that only one of each pair of face-sharing tetrahedral sites in hcp is occupied. All of the occupied tetrahedral sites point in the same direction, as shown in part b of Figure 1. The occupied tetrahedral sites share only corners, with the LiO_4 and FeO_4 tetrahedra each forming zigzag rows in directions parallel to the close-packed oxide−ion planes, as shown in part b of Figure 1. There are continuous Fe−O−Fe interactions throughout the structure, ensuring pathways for e^- transfer. Each LiO_4 tetrahedron shares three of its four faces with empty octahedral sites that bridge between neighboring LiO_4 tetrahedra, thus providing continuous tetrahedral−octahedral−tetrahedral pathways for Li^+ ion transport parallel to the close-packed oxide−ion planes. The fourth face of the tetrahedron, which is shared with a tetrahedron pointing in the opposite direction, perpendicular to the close-packed planes, provides a route for Li^+ ions to move perpendicular to the close-packed planes. Once in this tetrahedron, it may then migrate

(21) Matthewman, J. C.; Thompson, P.; Brown, P. J. *J. Appl. Crystallogr.* **1982**, *15*, 167.
(22) Sears, V. F. *Neutron News* **1992**, *3* (3), 26.
(23) Ufheil, J.; Baertsch, M. C.; Würsig, A.; Novák, P. *Electrochim. Acta* **2005**, *50*, 1733.
(24) Armstrong, A. R.; Holzapfel, M.; Novák, P.; Johnson, C. S.; Kang, S.-H.; Thackeray, M. M.; Bruce, P. G. *J. Am. Chem. Soc.* **2006**, *128*, 8694.
(25) Grey, I. E.; Hill, R. J.; Hewat, A. W. *Z. Kristallogr.* **1990**, *193*, 51.
(26) West, A. R.; Bruce, P. G. *Acta Crystallogr., Sect. B* **1982**, *38*, 1891.

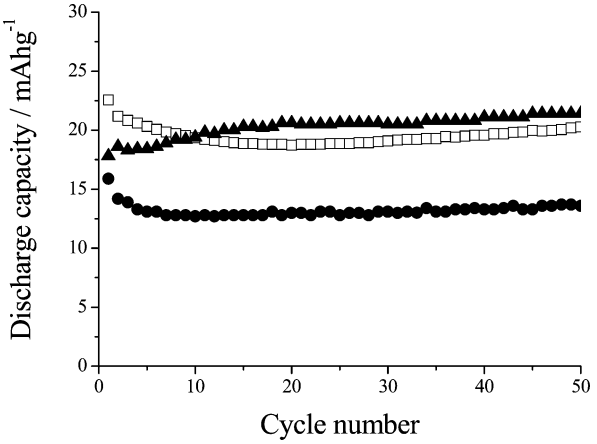

Figure 2. Variation of discharge capacities vs cycle number for as-prepared T−$LiFeO_2$. (□) cycled between 1.5−4.6 V at a rate of 25 mAg^{-1}, (●) cycled between 1.5−4.6 V at a rate of 100 mAg^{-1}, (▲) cycled between 1.5 and 4.95 V at a rate of 100 mAg^{-1}.

into a neighboring octahedron, thus Li^+ transport is possible in all directions within the structure. However, the electronic conductivity of T−$LiFeO_2$ was found to be similar to that of $LiFePO_4$ at around 10^{-9} S cm^{-1}.

There is a large family of compounds known as the tetrahedral structures, and several have been shown to support Li^+ transport. For example, LISICON, $Li_{2+2x}Zn_{1-x}GeO_4$, is an interstitial solid solution based on the stoichiometric compound Li_2ZnGeO_4, which adopts tetragonally packed oxide ions, with the Li_2ZnGe cations occupying half of the tetrahedral sites.[27−28] Although the cation ordering in LISICON is more closely related to that of the γ-$NaFeO_2$ polymorph than β, its high lithium-ion mobility demonstrates the significance of tetrahedral structures as ionic conductors. Recent interest in the lithium intercalation compound Li_2FeSiO_4, another closely related tetrahedral structure with tetragonally packed oxide ions, adds further emphasis to the significance of this family of compounds as electrodes and electrolytes.[29]

Electrochemistry of T−$LiFeO_2$. Electrodes were fabricated as described above. Even charging to 5.1 V versus Li^+ (1M)/lithium only leads to capacities around 20 $mAhg^{-1}$ on discharge, as shown in Figure 2. Changing the rate has a significant effect on the capacity, suggesting that the low capacities may be a function of kinetics.

In response to the above results, ball milling of the materials was investigated to reduce the particle size and address the kinetic limitations. Ball milling the ion-exchanged T−$LiFeO_2$ phase resulted in structural degradation, with the appearance of PXRD peaks corresponding to α-$LiFeO_2$ (a disordered rock-salt-based phase). Reasoning that the sodium phase may be more stable, we subjected β-$NaFeO_2$ to ball milling with subsequent ion exchange, resulting in single-phase T−$LiFeO_2$. Examination of TEM data indicated that the particle size of the non-ball-milled T−$LiFeO_2$ was already around 1 μ. After 2 h of ball-milling, the particle size was reduced to around 10 nm, as shown in part c of Figure 3, although there was considerable agglomeration of the small particles, as shown in part b of Figure 3. The electrochemical data for the ball-milled materials are

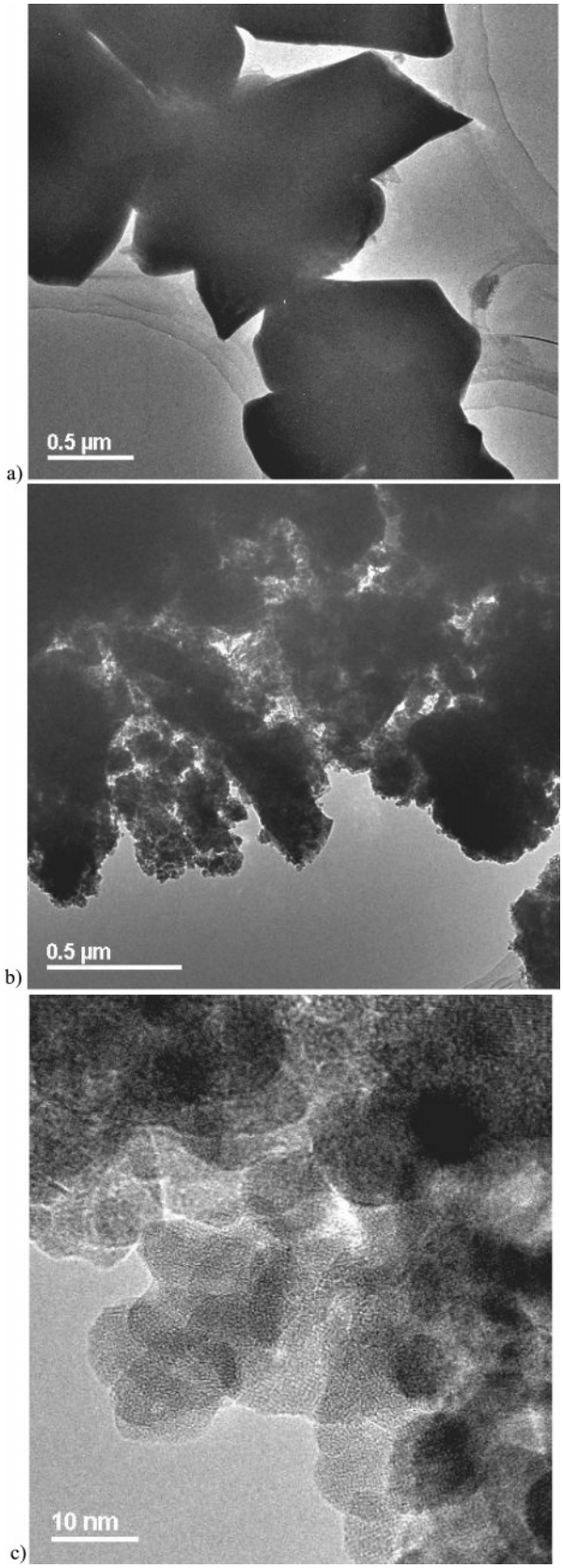

Figure 3. Transmission electron micrograph of (a) as-prepared T−$LiFeO_2$, (b) T−$LiFeO_2$ prepared from β-$NaFeO_2$ ball-milled for 2 h showing agglomeration of particles, (c) T−$LiFeO_2$ prepared from β-$NaFeO_2$ ball-milled for 2 h, showing individual particles.

presented in Figure 4. The significant increase in capacity on ball-milling is immediately evident. The capacities increased

(27) West, A. R.; Glasser, F. P. *J. Solid State Chem.* **1972**, *4*, 20.
(28) Hong, H. Y. P. *Mater. Res. Bull.* **1978**, *13*, 117.
(29) Nyten, A.; Abouimrane, A.; Armand, M.; Gustafsson, T.; Thomas, J. O. *Electrochem. Commun.* **2005**, *7*, 156.

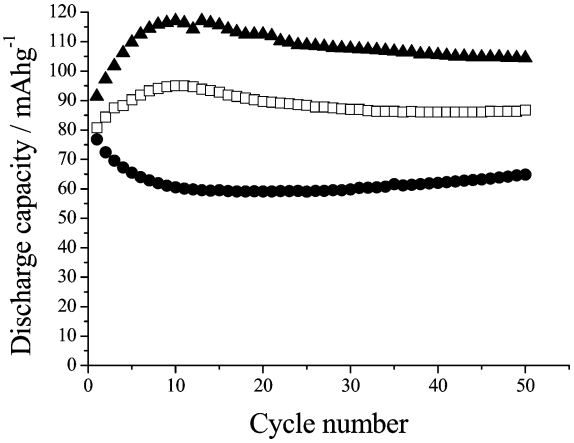

Figure 4. Variation of discharge capacities vs cycle number for T−$LiFeO_2$ synthesized from β-$NaFeO_2$ ball-milled for 2 h. (●) cycled between 1.5−4.6 V at a rate of 25 mAg^{-1}, (□) cycled between 1.5−4.95 V at a rate of 100 mAg^{-1}, (▲) cycled between 1.5 and 5.1 V at a rate of 100 mAg^{-1}.

with ball-milling of up to 2 h, and further milling resulted in partial decomposition. Figure 4 indicates that capacities as high as 120 mAhg^{-1} can be obtained at 100 mAg^{-1}, albeit over a wide voltage range of 1.5 to 5.1V. Capacity retention after the initial rise is quite good, as shown in Figure 4. The variation of the discharge capacities during the first few cycles is related to a change in the electrode structure.

The variation of potential with the state of charge is shown in Figure 5 for the 3 different upper cutoff potentials and for several cycles up to cycle number 50. The most dramatic change occurs during the first few cycles. After the first charge, most of the cycling occurs in a voltage range more compatible with the Fe^{2+}/Fe^{3+} couple than Fe^{3+}/Fe^{4+}. Such changes in shape and potential on cycling usually signal a transformation in the structure, in accordance with the variation in the discharge capacities over the same early cycles, as shown in Figure 4. XANES data collected at the end of charge reveal no evidence for Fe^{4+}, only Fe^{3+}, confirming the absence of a simple redox process. It should be noted that the first discharge capacity exceeds the first charge, implying formation of Fe^{2+} at the end of the discharge. Attempts to insert lithium into as-prepared $LiFeO_2$ (i.e., to commence with discharge rather than charge) resulted in a similar 30−40 mAhg^{-1} (excess) discharge capacity, indicating that the host material can accommodate a small amount of lithium (10−15%). To further investigate a possible structural transformation on cycling, PXRD data were collected as a function of cycle number, as shown in Figure 6. Comparing the PXRD data after various cycle numbers, it is evident that changes occur on extended cycling, especially in the regions around 55 and 82° in 2θ ($FeK_{\alpha 1}$), with new peaks growing in these regions. Comparison of these data with the JCPDS database did not provide a definitive interpretation of the additional peaks. To clarify the situation, a cell was arrested at the end of the charge after 20 cycles. The PXRD data from this cell are included in Figure 6. The principal lines for the defect spinel $LiFe_5O_8$, from the JCPDS database, are also included in the figure and exhibit a good match to the additional peaks in the PXRD data, demonstrating that on cycling the structure converts from tetrahedral $LiFeO_2$ (distorted hcp packing) to the defect spinel $LiFe_5O_8$ (ccp packing). It has been reported that $LiFe_5O_8$ may be cycled between this composition and compositions that can approach $Li_5Fe_5O_8$, associated with the Fe^{2+}/Fe^{3+} redox couple, thus explaining the evolution of the voltage versus state of charge plots, in Figure 5, to lower voltages on cycling.[30]

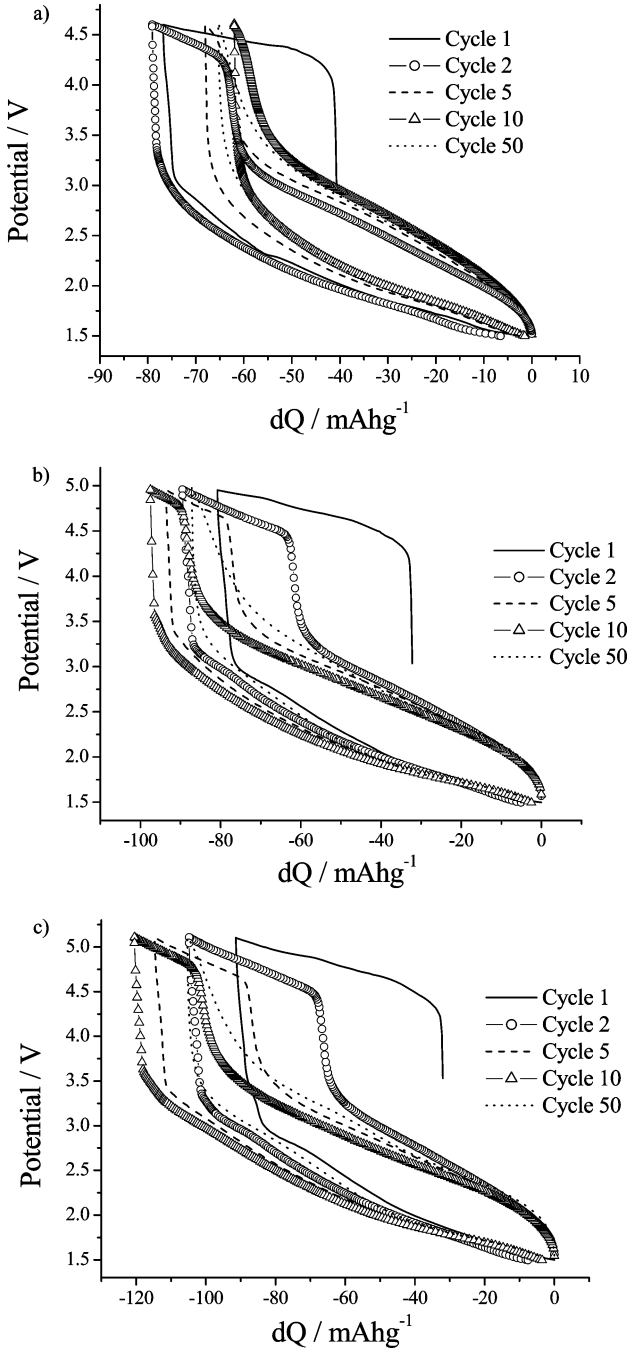

Figure 5. Charge−discharge voltage profiles for T−$LiFeO_2$ synthesized from β-$NaFeO_2$ ball-milled for 2 h. (a) Cycled 1.5−4.6 V at a rate of 25 mAg^{-1}, (b) cycled 1.5−4.95 V at 100 mAg^{-1}, and (c) cycled 1.5−5.1 V at 100 mAg^{-1}.

The transformation from T−$LiFeO_2$ to $LiFe_5O_8$ ($Li_{0.2}FeO_{1.6}$) on cycling must involve the overall loss of oxygen from the material; how then does this process occur? Such oxygen loss could take place by direct evolution of O_2 from $LiFeO_2$ during charging above 4.5 V. This has been observed before for manganese-based oxides, for example, the layered $Li[Li_{0.2}Ni_{0.2}Mn_{0.6}]O_2$, where oxidation beyond the point in which manganese and nickel are both in the +4 oxidation state, is accompanied

(30) Chen, C. J.; Greenblatt, M.; Waszczak, J. V. *J. Solid State Chem.* **1986**, *64*, 240.

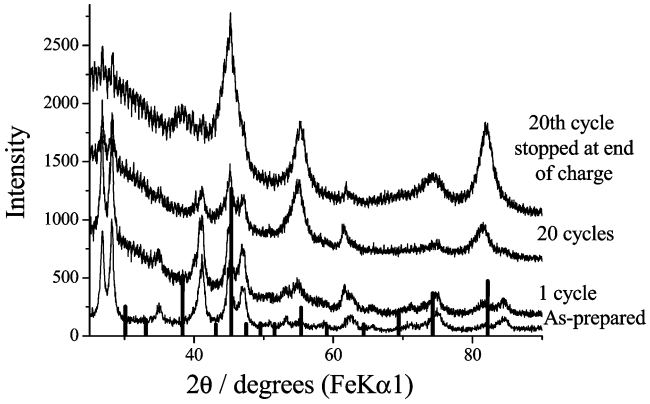

Figure 6. Powder X-ray diffraction patterns for T−$LiFeO_2$ as a function of electrochemical cycling. Tick marks show peak positions for $LiFe_5O_8$.

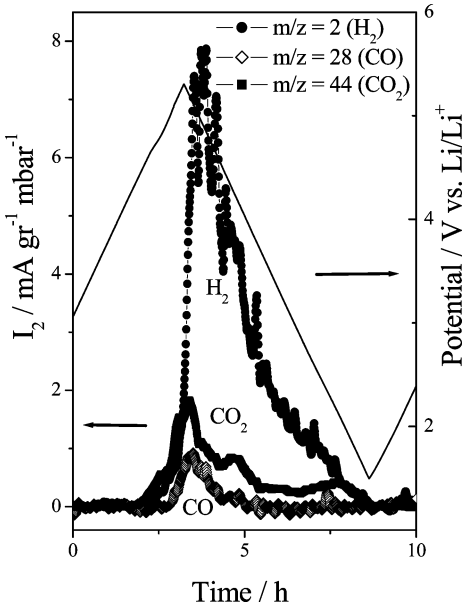

Figure 7. DEMS trace for T−$LiFeO_2$ showing traces for H_2, CO, and CO_2.

by O_2 evolution.[31] Alternatively, direct electrolyte oxidation may occur as observed on charging Li_2MnO_3 at elevated temperatures.[32] To address this issue, cells were cycled and the gases evolved from the cell during charge and discharge measured in-situ by differential electrochemical mass spectrometry (DEMS). The technique is described elsewhere.[33,34] The results are presented in Figure 7. There is little evidence of O_2 gas evolution on charging during the first or subsequent cycles. However, significant CO_2 and CO evolution was evident on charging at high voltages, as shown in Figure 7. It has been shown previously that evolution of such gases from $LiPF_6$ in EC/DMC is indicative of electrolyte oxidation.[33,34] As soon as discharge commences, gas evolution is dominated by H_2, as shown in Figure 7. It is known that electrolyte oxidation may be accompanied by the generation of H^+.[35] Summarizing the DEMS results, they point to electrolyte oxidation accompanying charging.

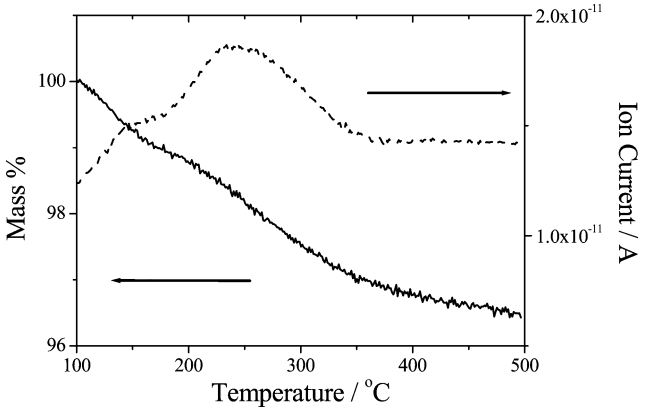

Figure 8. Thermogravimetric analysis (solid line) and mass spectrometry (dashed line) traces for a $LiFeO_2$ electrode charged to 5.1 V, heated under argon at 5 °C/min.

A charged electrode was removed from the cell in the glovebox, carefully washed with dimethyl carbonate, dried, and transferred to a thermogravimetric analyzer coupled with mass spectrometry. The TG-MS measurement was carried out under argon. The results are shown in Figure 8, from which H_2O evolution on heating at 150 and 250 °C is evident, demonstrating the presence of H^+ in the charged material. Considering all of the results together, no evidence of Fe^{3+} oxidation to Fe^{4+} on charging, the lack of direct O_2 evolution, evidence for electrolyte decomposition, and the presence of a significant amount of hydrogen in the electrode at the end of the charge, a possible mechanism for the conversion of T−$LiFeO_2$ to $LiFe_5O_8$ may be proposed. We suggest that electrolyte oxidation on charging above approximately 4.6 V is accompanied by the generation of H^+, which exchanges for Li^+ in $LiFeO_2$

$$LiFeO_2 + xH^+ \rightarrow Li_{(1-x)}H_xFeO_2 + xLi^+$$

followed by the leaching of H_2O from the material (effective removal of hydrogen and oxygen), as has been noted previously, e.g., from $Li_{2-x}H_xMnO_3$.[36−38] Although this mechanism fits the results, it remains speculative; however, there is no doubt that oxygen is lost and not by direct evolution.

In conclusion, $LiFeO_2$ with tetrahedral Fe^{3+} has been synthesized for the first time and its structure refined, showing that it corresponds to the β-polymorph of $NaFeO_2$, from which it was formed by ion exchange. Lithium may be removed from this compound, and capacities of 120 $mAhg^{-1}$ at a rate of 100 mAg^{-1} may be obtained over a wide voltage range and with reasonable capacity retention on cycling. Cycling is accompanied by transformation of the tetragonally close-packed structure to that of the cubic close-packed defect spinel $LiFe_5O_8$. The process involves oxygen loss, but in situ differential electrochemical mass spectrometry shows that this is not accompanied by direct evolution of O_2 gas, as has been observed for some manganese materials. It does however demonstrate that electrolyte oxidation accompanies charging. Such results, together with TG-MS data that indicate the presence of hydrogen in the material after charging, leads to a possible mechanism of oxygen loss. We suggest that electrolyte oxidation on charging is

(31) Armstrong, A. R.; Holzapfel, M.; Novak, P.; Johnson, C. S.; Kang, S-H.; Thackeray, M. M.; Bruce, P. G. *J. Am. Chem. Soc.* **2006**, *128*, 8694.
(32) Robertson, A. D.; Bruce, P. G. *Chem. Mater.* **2003**, *15*, 1984.
(33) Imhof, R.; Novák, P. *J. Electrochem. Soc.* **1999**, *146*, 1702.
(34) Ufheil, J.; Würsig, A.; Schneider, O. D.; Novák, P. *Electrochem. Commun.* **2005**, *7*, 1380.
(35) Du Pasquier, A.; Blyr, A.; Courjal, P.; Larcher, D.; Amatucci, G.; Gérand, B.; Tarascon, J. M. *J. Electrochem. Soc.* **1999**, *146*, 428.
(36) Thackeray, M. M.; Johnson, C. S.; Vaughey, J. T.; Li, N.; Hackney, S. A. *J. Mater. Chem.* **2005**, *15*, 2257.
(37) Rossouw, M. H.; Thackeray, M. M. *Mater. Res. Bull.* **1991**, *26*, 463.
(38) Rossouw, M. H.; Liles, D. C.; Thackeray, M. M. *J. Solid State Chem.* **1993**, *104*, 464.

accompanied by H^+ generation, which exchanges for Li^+ in T−$LiFeO_2$, forming $Li_{1-x}H_xFeO_2$. This in turn loses H_2O, resulting in the overall loss of oxygen from T−$LiFeO_2$ to form $LiFe_5O_8$. This is the first study of the electrochemistry of a tetrahedral $LiFeO_2$ compound. Despite Fe^{3+} being in tetrahedral rather than octahedral coordination, (all of the previous $LiFeO_2$ compounds contained Fe^{3+} in octahedral coordination) and despite the O^{2-} packing being closer to hcp than ccp, the T−$LiFeO_2$ phase has proven to be unstable on cycling, rendering it unusable for practical applications. Future studies will be devoted to modifying or doping $LiFeO_2$ to investigate the influence of such strategies on its structural stability and electrochemical performance.

Acknowledgment. PGB thanks the EPSRC for financial support.

Supporting Information Available: Graphs of the refined neutron diffraction pattern for T-$LiFeO_2$ and of XANES spectra for T-$LiFeO_2$ at the end of charge. This material is available free of charge via the Internet at http://pubs.acs.org.

JA077651G